Posterior (Outward) Migration of the Lamina Cribrosa and Early Cupping in Monkey Experimental Glaucoma

Hongli Yang,[1] *Galen Williams,*[1] *J. Crawford Downs,*[2] *Ian A. Sigal,*[2,3] *Michael D. Roberts,*[2] *Hilary Thompson,*[4] *and Claude F. Burgoyne*[1]

Purpose. To quantify the lamina cribrosa insertion into the peripapillary sclera and optic nerve pia in normal (N) and early experimental glaucoma (EEG) monkey eyes.

Methods. Perfusion-fixed optic nerve heads (ONHs) from 21 animals were digitally reconstructed three dimensionally and delineated. *Anterior Laminar Insertion Position (ALIP), Posterior Laminar Insertion Position (PLIP), Laminar Insertion Length (LIL;* distance between the anterior and posterior laminar insertions), and *Scleral Thickness* (at the Anterior Subarachnoid space) were calculated for each ONH. Animals were pooled into four groups based on the kill condition (N vs. EEG) and perfusion IOP (10, 30, or 45 mm Hg) of each eye: N10-N10 ($n = 6$), N30/45-N10 ($n = 6$), EEG10-N10 ($n = 3$), and EEG30/45-N10 ($n = 6$). Glaucomatous EEG versus N eye differences in each group and each animal were required not only to achieve statistical significance ($P < 0.05$) but also to exceed physiologic intereye differences within the bilaterally normal groups.

Results. ALIP was significantly posterior (outward) in the EEG compared with N10 eyes of the EEG30/45-N10 group and 5 of 9 individual EEG eyes (difference range, 12–49 μm). PLIP was significantly posterior in the EEG eyes of both EEG groups and in 6 of 9 individual EEG eyes (range, 25–83 μm). LIL ranged from 90 to 190 μm in normal eyes and was significantly increased within the EEG eyes of both EEG groups and in 7 of 9 individual EEG eyes (difference range, 30–47 μm).

Conclusions. Posterior migration of the lamina cribrosa is a component of early cupping in monkey EEG. (*Invest Ophthalmol Vis Sci.* 2011;52:7109–7121) DOI:10.1167/iovs.11-7448

Cupping is a clinical term used to describe enlargement of the optic nerve head (ONH; Table 1) cup in all forms of optic neuropathy.[1] However, cupping is also used as a synonym for the pathophysiology of glaucomatous damage to the ONH neural and connective tissues.[2,3] Because the clinical and pathophysiologic contexts for cupping are seldom clarified, there is a large and often confusing literature regarding the presence and importance of cupping in a variety of optic neuropathies, including glaucoma.[4] Within the context of this discussion, the unique features of a glaucomatous form of cupping have yet to be agreed on.[5–7]

We have previously proposed[6] that the clinical phenomenon of cupping has two principal pathophysiologic components in all optic neuropathies: prelaminar thinning and laminar deformation. We define prelaminar thinning to be the portion of cup enlargement that results from thinning of the prelaminar tissues caused by physical compression and/or loss of retinal ganglion cell (RGC) axons. We define laminar deformation or laminar cupping to be the portion of cup enlargement that results from permanent, IOP-induced deformation[7–14] of the lamina cribrosa and peripapillary scleral connective tissues after damage, remodeling, or both.[15–17]

Although histologic sections from a small number of human[18,19] and monkey[20] eyes with early glaucoma have been included in previous reports, there has been no systematic description of the transition from ocular hypertension to early glaucomatous cupping in either monkey or human cadaver eyes. In monkeys, we have previously reported that laminar and peripapillary scleral deformation and laminar thickening underlie the onset of confocal scanning laser tomography (CSLT)-detected cupping in nine young adult monkey eyes exposed to moderate experimental IOP elevations.[12] We have also presented evidence to support regional laminar beam thickening and thinning (Grimm J, et al. *IOVS* 2007;48:ARVO E-Abstract 3295) and retrolaminar septal recruitment into the lamina[21,22] in 3 of these 9 early experimental glaucoma (EEG) eyes.

The purpose of the present study was to test the hypothesis that in addition to ONH connective tissue deformation and thickening, early glaucomatous cupping in the EEG eye of these same nine animals included posterior migration of the lamina cribrosa from the sclera toward (and, in some cases, into) the pial sheath[17,23] (Yang H, et al. *IOVS* 2010;51:ARVO E-Abstract 1631). To do so, we quantified the anterior (inner) and posterior (outer) lamina cribrosa insertions (Fig 1) relative to the scleral canal opening within 3D histomorphometric reconstructions of both eyes of the same nine (EEG) monkeys and compared the intereye differences within the EEG animals to a second group of 12 bilaterally normal animals from two previous reports.[13,14] We specifically proposed that progressive posterior laminar migration in the EEG eyes, if present, would manifest as two findings within the postmortem reconstructions: first, posterior displacement of the anterior and posterior laminar insertions (respectively) within the EEG eyes relative to their contralateral normal control eyes; second, EEG to normal eye differences in the EEG animals that exceeded the

From the [1]Optic Nerve Head Research Laboratory and the [2]Ocular Biomechanics Laboratory, Devers Eye Institute, Legacy Health System, Portland, Oregon; [3]Ocular Biomechanics Laboratory, Department of Ophthalmology, University of Pittsburgh Medical Center, Pittsburgh, Pennsylvania; and [4]School of Public Health, Louisiana State University Health Sciences Center, New Orleans, Louisiana.

Supported in part by United States Public Health Service Grant R01EY011610 (CFB); the American Health Assistance Foundation (CFB); The Whitaker Foundation (CFB); a Career Development Award from the American Glaucoma Society (CFB); The Legacy Good Samaritan Foundation, Portland, Oregon; the Sears Trust for Biomedical Research, Mexico, Missouri; and the Alcon Research Institute, Fort Worth, Texas.

Submitted for publication February 24, 2011; revised May 11, 2011; accepted May 28, 2011.

Disclosure: **H. Yang**, None; **G. Williams**, None; **J.C. Downs**, None; **I.A. Sigal**, None; **M.D. Roberts**, None; **H. Thompson**, None; **C.F. Burgoyne**, None

Corresponding author: Claude F. Burgoyne, Optic Nerve Head Research Laboratory, Devers Eye Institute, 1225 NE Second Avenue, Portland, OR 97232; cfburgoyne@deverseye.org.

TABLE 1. Acronyms

Acronym	Full Name
ALI	Anterior Laminar Insertion; see Figures 1 and 2
*ALIP**	*Anterior Laminar Insertion Position*
ANOVA	Analysis of variance
ASAS	Anterior-most Subarachnoid Space; see Figures 1 and 2
ASCO	Anterior Scleral Canal Opening; see Figures 1 and 2
BMO	Bruch's Membrane Opening; see Figures 1 and 2
CSLT	Confocal Scanning Laser Tomography
EEG	Early Experimental Glaucoma
EEG10	EEG10 eyes of the EEG10-N10 group
EEG30/45	EEG30/45 eyes of the EEG30/45-N10 group
EEG10-N10	EEG10 vs. N10 group; $n = 3$ animals
EEG30/45-N10	EEG30/45 vs. N10 group; $n = 6$ animals
*LIL**	*Laminar Insertion Length*
N	Normal
N10	N10 eyes of any of the four groups
N30/45	N30/45 eyes of the N30/45-N10 group
N10-N10	N10 vs. N10 group; $n = 6$ animals
N30/45-N10	N30/45 vs. N10 group; $n = 6$ animals
ONH	Optic Nerve Head
PLI	Posterior Laminar Insertion; see Figures 1 and 2
*PLIP**	*Posterior Laminar Insertion Position*
PSCO	Posterior Scleral Canal Opening; see Figures 1 and 2

* Laminar insertion measurement parameters are italicized to distinguish them from anatomic landmarks.

physiologic intereye differences within the bilaterally normal animals.

The concept that early glaucomatous cupping includes posterior migration of the lamina cribrosa is important for the following reasons. First, posterior migration of the anterior laminar insertion (Figs. 2A, 2B), considered alone, requires either physical disruption[7,19] or remodeling[15,16] of the anterior laminar beams and their contained capillaries, providing credible mechanisms for the phenomenon of glaucomatous excavation[18,19] and glaucomatous optic disc hemorrhages.[24,25] Second, posterior migration of the posterior laminar insertion (Figs. 2C, 2D) that includes recruitment of the retrolaminar septa[22] suggests that at least a portion of glaucomatous cupping may be a protective connective tissue remodeling response to an altered and challenging biomechanical environment.[15,17,26,27] Third, posterior migration of the anterior and posterior laminar insertions (Fig. 2) should alter the blood supply of the laminar beams,[28] the steepness of the translaminar pressure gradient,[29–33] and astrocyte and axonal physiology[15,34,35] within the peripheral neural canal, where the RGC axons are thought to be most susceptible to axon transport disruption.[36,37] Fourth, clinical detection of laminar migration may provide early evidence for glaucomatous ONH change and may soon be possible using spectral domain optical coherence tomography (OCT)[38,39] or adaptive optics OCT[40] of the ONH.

Table 1 includes the definitions of all acronyms used in this article.

MATERIALS AND METHODS

Animals

All animals were treated in accordance with the ARVO Statement for the Use of Animals in Ophthalmic and Vision Research. Twenty-one monkeys were used for this study (Table 2) and have been extensively characterized in a series of previous reports.[6,8,9,12–14] The monkeys were divided into four groups reflecting the kill condition (normal [N] vs. EEG) and IOP (10, 30, or 45 mm Hg) at the time of perfusion: N10-N10, $n = 6$ bilaterally normal animals, each perfusion fixed with both eyes set to IOP 10 mm Hg by anterior chamber manometer; N30/45-N10, $n = 6$ bilaterally normal animals, each perfusion fixed with one eye set to either IOP 30 or 45 mm Hg and the other eye set to IOP 10 mm Hg by anterior chamber manometer[13]; EEG10-N10 group, $n = 3$ animals, each perfusion fixed with both the normal and the EEG eye set to IOP 10 mm Hg by anterior chamber manometer; EEG30/45-N10, $n = 6$ animals, each perfusion fixed with the EEG eye set to IOP 30 or 45 mm Hg and the normal eye set to IOP 10 mm Hg by anterior chamber manometer.

Early Experimental Glaucoma, ONH Surface Imaging, and Cumulative IOP Insult

We have previously described the use of CSLT and our CSLT parameter, mean position of the disc, to detect the onset of the ONH surface in monkey EEG.[10,11] All CSLT imaging in these animals was performed using a topographic scanning system (TopSS; Laser Diagnostics Technology, San Diego, CA). After three to eight baseline testing sessions, one eye of each monkey was submitted to laser-induced experimental IOP elevation, after which CSLT imaging of both eyes was repeated at 2-week intervals until the onset of a qualitative decrease in mean position of disc on two successive post-laser imaging sessions.[12]

All EEG monkeys were killed within approximately 1 to 5 weeks of CSLT detection of ONH surface change.[12] Within the nine EEG eyes, this occurred after 2 to 18 weeks of moderate IOP elevation. Cumulative IOP difference was calculated for each EEG eye, as described in Table 2.

Monkey Euthanatization and Perfusion Fixation at Prescribed IOP

We have previously described our perfusion fixation method.[9–11] Briefly, IOP in both eyes of each animal was set to 10 mm Hg for at least 30 minutes. For the N10-N10 and EEG10-N10 groups, each animal was then perfusion fixed under deep pentobarbital anesthesia through the descending aorta with 1 L of 4% buffered hypertonic paraformaldehyde solution, followed by 6 L of 5% buffered hypertonic glutaraldehyde solution. For the animals in which one eye was fixed at 30 or 45 mm Hg, IOP was elevated for at least 15 minutes before perfusion fixation was initiated. After perfusion fixation, target IOP was maintained for 1 hour, at which time both eyes were enucleated, all extraocular tissues were removed, and the intact anterior chamber was excised 2 to 3 mm posterior to the limbus. By gross inspection, perfusion was excellent in all eyes fixed at 10 mm Hg IOP. However, blood was variably present in the retinal vessels, posterior ciliary arteries and vortex veins of the high IOP eyes. The posterior scleral shell with intact ONH, choroid, and retina were then placed in 5% glutaraldehyde solution for storage.

3D Histomorphometric Reconstruction

For each eye, the ONH and peripapillary sclera were trephined (6-mm-diameter), pierced with alignment sutures, and embedded in paraffin. The block was then mounted on a microtome and serial sectioned at 3-μm thickness[10] (1.5 μm in N10-N10 group using an enhanced protocol)[14] from the vitreous surface through the ONH into the orbital optic nerve. After each section was taken, the block surface was stained with a 1:1 (vol/vol) mixture of Ponceau S and acid fuchsin, then imaged at a resolution of 2.5 $\times$ 2.5 μm per pixel[10] (1.5 $\times$ 1.5 μm in the N10-N10 group).[14] Serial section images for each ONH were then aligned in the anterior-to-posterior direction using the sutures as fiduciary markers and stacked into a 3D reconstruction of the ONH and peripapillary scleral tissues.

Initial 3D Delineation of ONH and Peripapillary Scleral Landmark Points

Within 40 digital radial sagittal section images of the 3D digital histomorphometric reconstruction (Fig. 3), the delineator marked seven surfaces and six pairs of neural canal landmarks (Figs. 1, 3). The seven

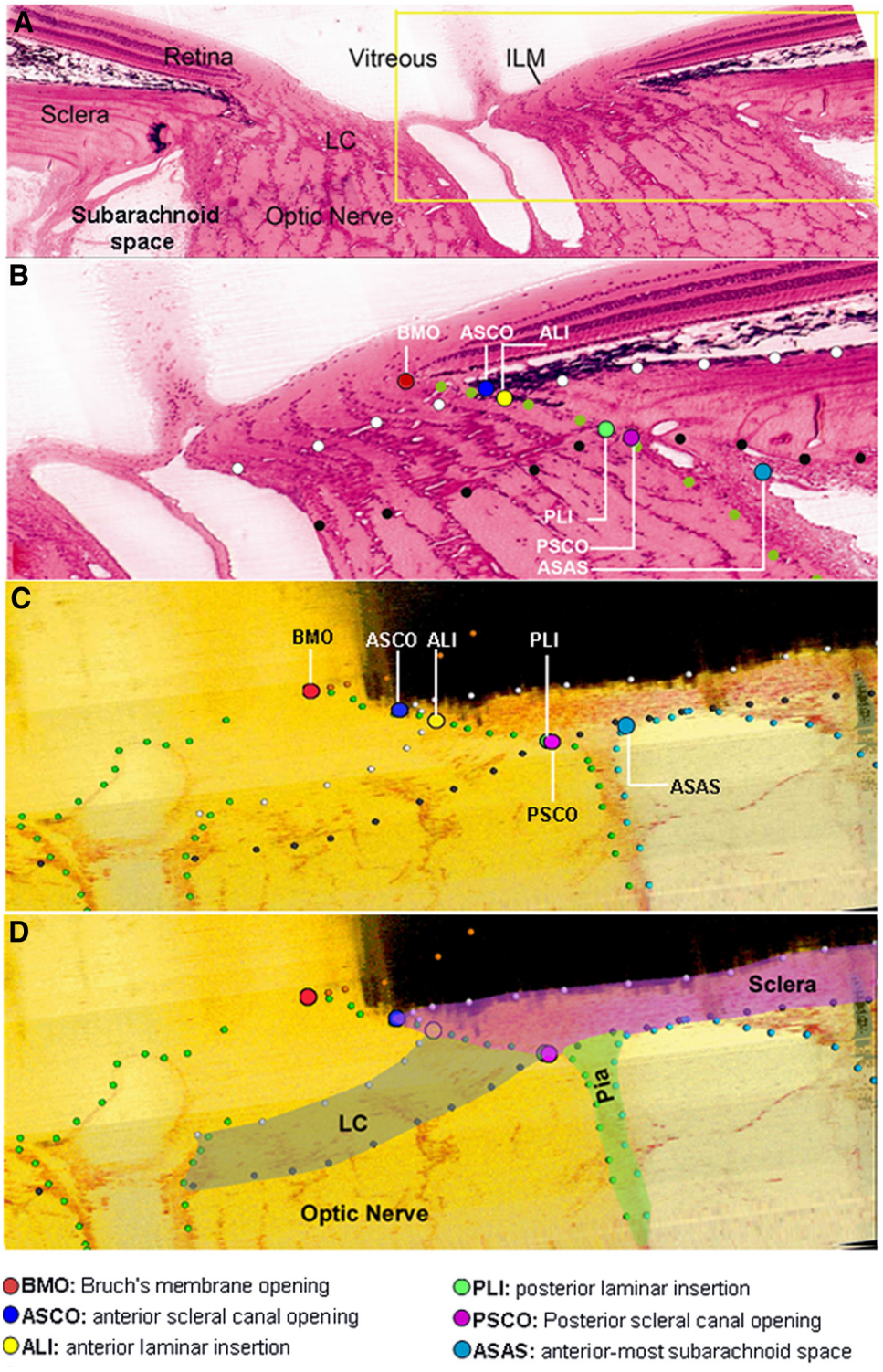

FIGURE 1. Neural canal landmarks within a representative histologic section (**A**, **B**) and a representative digital sagittal section (**C**, **D**) of a 3D histomorphometric ONH reconstruction. (**A**) Digital image of a representative central horizontal histologic section from a normal monkey eye perfusion fixed at an IOP of 10 mm Hg with the nasal side of the canal magnified in (**B**) (note that these histologic sections are included to clarify the anatomic relationships seen in **C**; no histologic sections were used in this study). (**C**) The nasal portion of a representative digital horizontal sagittal section of a normal monkey ONH 3D histomorphometric reconstruction showing the marks for seven landmark surfaces and six pairs of landmark points that were 3D-delineated using linked, simultaneous colocalization of each delineated point within its radial sagittal and transverse section images. The principal neural canal landmarks (**B**, **C**) are depicted in color (see legend below the figure). Additional ONH landmark and surface points are as follows: anterior laminar/scleral surface, *white*; posterior laminar/scleral surface, *black*; neural boundary, *light green.* Neural boundary points from all 40 radial sections of the 3D histomorphometric volume images were used to create the neural boundary surface seen in Figure 4. The border tissues of Elschnig are not separately delineated but are simply the portion of the neural canal boundary that extends from the ASCO to the BMO (**C**). (**D**) Sclera, LC, and pia are segmented using different colors. The posterior scleral surface is the biologically continuous interface that separates the dense horizontally organized sclera from the perpendicularly oriented pial and dural tissues (not completely shown) and the more loosely organized episcleral tissues.

delineated surfaces included the internal limiting membrane, Bruch's membrane, the anterior and posterior lamina cribrosa surfaces, the anterior and posterior scleral surfaces, and the neural canal boundary. The following neural canal landmark points were delineated (Figs. 1B, 1C): Bruch's membrane opening (BMO), anterior scleral canal opening (ASCO), anterior laminar insertion (ALI), posterior laminar insertion (PLI), posterior scleral canal opening (PSCO), and anterior-most aspect of the subarachnoid space (ASAS). Three experienced delineators performed all the delineations in this study, and a single one delineated both eyes of each animal. Delineators were not masked to the IOP or kill condition of each eye. On completion of delineation, the marks were checked for accuracy by two experienced observers (HY and CFB).

Laminar Insertion Parameterization within a Second Series of Digital Sections Centered on BMO

Because the most consistent and statistically robust characterization of this anatomy (within and between eyes) would be based on equally

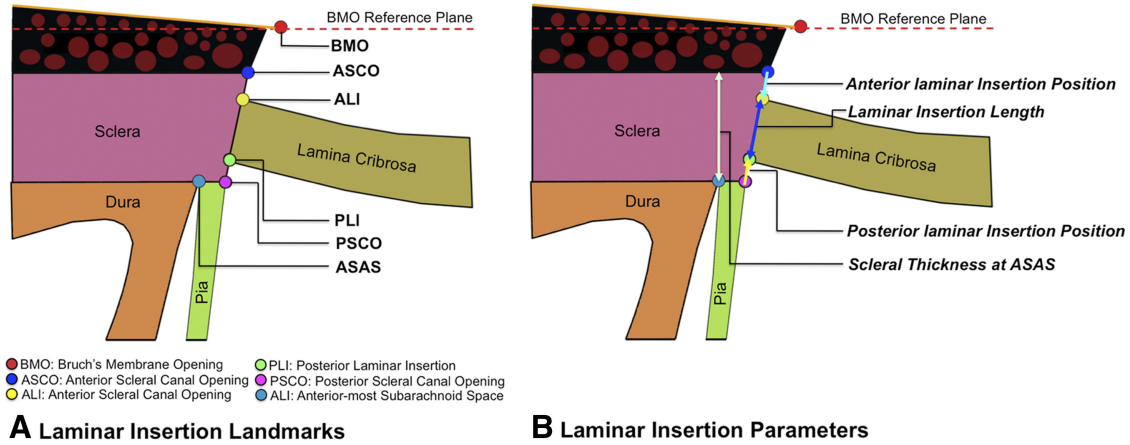

Figure 2. Four laminar insertion parameters. The principal laminar insertion landmarks (depicted within a histologic section and a digital histomorphometric section image) are schematically depicted (**A**). Four laminar insertion parameters are depicted (**B**) and are italicized throughout the manuscript to distinguish them from the landmarks they measure. *ALIP* is the position of the ALI relative to the ASCO. *ALIP* is positive (not shown) when the anterior lamina inserts into the border tissues of Elshnig (described here) and negative (*cyan arrow*) when the anterior lamina inserts into the sclera. *PLIP* is the position of the PLI relative to the ASCO. *PLIP* is positive (*yellow arrow*) when the posterior lamina inserts to the sclera and negative when the posterior lamina inserts to the pia (shown in Fig. 5B, left). *LIL* is the distance between the anterior and posterior laminar insertions (*blue arrow*). *Scleral Thickness at ASAS* (*light green arrow*) is the minimum scleral thickness measured from the anterior-most aspect of the subarachnoid space.

spaced measurements within true perpendicular sections, the initial delineations described above were digitally resampled as follows. For each 3D ONH reconstruction, ASCO, ALI, PSCO, and PLI landmarks (2 points in each of the 40 radial digital section images or 80 points for each landmark) were fitted with B-spline curves, as shown in Figure 4. A plane satisfying a minimum sum-of-squared-error criterion was fit to the 80 BMO points, thereby creating a BMO reference plane (Fig. 4C).[9,41] A second set of 40 radial digital sections centered on the BMO centroid and perpendicular to the BMO reference plane was then obtained (Fig. 4).

The following parameters were quantified within each digital section (Fig. 2): *Anterior Laminar Insertion Position (ALIP),* defined as the position of the ALI relative to the ASCO; *Posterior Laminar Insertion Position (PLIP),* defined as the position of the PLI relative to the PSCO; *Laminar Insertion Length (LIL),* defined as the distance from the ALI to the PLI; and *Scleral Thickness at ASAS,* defined as the minimum distance between posterior scleral surface at the ASAS and the anterior scleral surface. We italicize and capitalize these parameters to distinguish their behavior from the behavior of the underlying anatomic landmarks, which are not italicized or capitalized.

Statistical Analyses

Overall data for each parameter by group and between the two eyes of each monkey were assessed by a factorial analysis of variance (ANOVA). Statistically significant differences within each group and between the two eyes of each animal required an overall significant

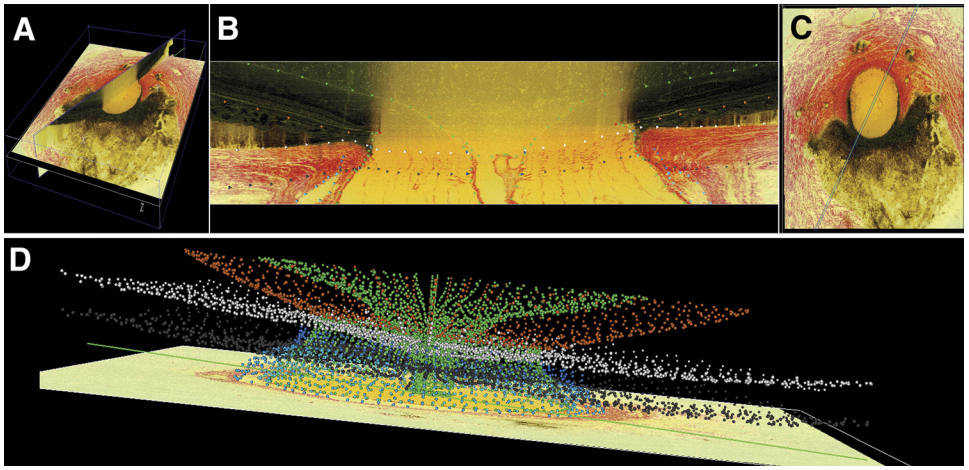

Figure 3. Initial 3D delineation within the colorized, stacked-section, 3D ONH reconstruction of a single ONH.[13] (**A**) A total of 40 serial digital radial sagittal sections, each 7 voxels thick, are served to the delineator at 4.5° intervals. (**B**) Representative digital sagittal slice showing all 13 3D-delineated landmarks. Delineation is performed using linked, simultaneous colocalization of the sagittal slice (shown) and the transverse section image through a given delineated point (**C**). (**D**) Representative 3D point cloud showing all delineated points for a normal monkey ONH relative to the posterior serial section image (vitreous, *top*; orbital optic nerve, *bottom*). For the purposes of this report, it should be noted that the 40 serial digital radial sagittal sections that were generated for 3D delineation of the standard ONH landmarks were centered on the operator's best estimate of the center of the ONH and perpendicular to the surface of the volumetric data set, which was not necessarily the same as being perpendicular to the sclera. To perform the parameterization necessary to test hypotheses regarding laminar insertion migration and pialization, we wanted to ensure that measurements were equally distributed around the canal and that they were made within digital sections that were as perpendicular to the structures being measured as could be obtained. Therefore, the point clouds above were surfaced and an ellipse was fit to the 80 delineated BMO points, allowing a separate set of 40 digital radial sections centered on the BMO ellipse centroid and perpendicular to the BMO reference plane to be obtained. This process is further explained in Figure 4. This figure previously published in Yang H, Downs JC, Sigal IA, Roberts MD, Thompson H, Burgoyne CF. Deformation of the normal monkey optic nerve head connective tissue after acute IOP elevation within 3D histomorphometric reconstructions. *Invest Ophthalmol Vis Sci.* 2009;50:5785–5799. © ARVO.

TABLE 2. Animal Data by Group

Group	Number of Animals	Age Mean (Range)*	Species	Sex	Eye Status	IOP at Baseline Mean (Range)	EEG Eye Post-laser Maximum IOP Mean (Range)	Cumulative IOP Difference†	IOP during Perfusion Fixation	Pre-euthanatization IOP Elevation Time (mins)
N10 - N10	6	7 (2–10)	R	3M/3F	N OD	12 (8–14)	N/A		10 mm Hg	N/A
					N OS	11 (8–14)	N/A	N/A	10 mm Hg	N/A
N30/45 - N10	6	7.5 (5–14)	5R/1C	5M/1F	N OD	9 (4–12)	N/A		30 or 45 mm Hg	15 or 30
					N OS	9 (4–12)	N/A	N/A	10 mm Hg	N/A
EEG10 - N10	3	10 (8–11)	C	M	N	10 (8–11)	N/A		10 mm Hg	N/A
					EEG	9 (9–10)	28 (20–37)	221 (116–360)	10 mm Hg	N/A
EEG30/45 - N10	6	8 (5–11)	4R/2C	M	N	10 (8–13)	N/A		10 mm Hg	N/A
					EEG	11 (8–14)	28 (16–38)	295 (50–807)	30 or 45 mm Hg	15

Animals in this study aged 7 (3 ~ 14; 16 young adults, 5 adults) during their period of study and aged 8 (3 ~ 14; 8 young adults and 13 adults) at the time of euthanatization. We defined young adults from age 3 to 8 and adults from 8 to 18. Axon loss for EEG10 - N10 monkeys ranged from 16 to 30%.[6] R, rhesus; C, cynomolgus; M, male; F, female; N/A, not applicable.

* Age at euthanatization.

† Cumulative IOP Difference is the difference in area under the IOP-time curve between the EEG and normal eye (units mm Hg days).

F-test followed by *t*-tests using $P < 0.05$ and corrected for multiple comparisons.[42]

For parameter comparison between the glaucoma or high IOP and control eyes of each group, we added the following empiric criteria to identify those statistically significant differences that most likely represent important biological differences. First, to account for physiologic intereye differences, we defined glaucomatous differences between the EEG10 and N10 eyes of the EEG10-N10 group to be only those statistically significant differences that exceeded the intereye difference within the N10-N10 group. We defined acute IOP-related differences between the N30/45 and N10 eyes of the N30/45-N10 group in the same manner.

To account for both physiologic intereye differences and the potential effects of acute IOP elevation just before perfusion fixation, we defined glaucomatous differences between the EEG30/45 and N10 eyes of the EEG30/45-N10 group to be only those statistically significant differences that exceeded the intereye differences within the N30/45-N10 group and within the N10-N10 group.

Similar to the overall data, for parameter comparisons between the treated and control eyes of each monkey we added additional empiric criteria to identify those statistically significant differences between the two eyes of each monkey that most likely represent important biological differences.[14] First, we defined glaucomatous differences between the EEG10 and N10 eyes of each EEG10-N10 animal to be only those statistically significant differences that exceeded the maximum physiologic intereye difference within the six animals of the N10-N10 group.[14] We defined acute IOP-related differences between the N30/45 and N10 eyes of each N30/45-N10 animal in the same manner. To account for both physiologic intereye differences and the potential effects of acute IOP elevation just before perfusion fixation, we defined glaucomatous differences between the EEG30/45 and N10 eyes of each EEG30/45-N10 animal to be only those statistically significant differences that exceeded the maximum physiologic intereye difference within the six animals of the N30/45-N10 group and six animals within the N10-N10 group.

RESULTS

Descriptive Data

A total of 15 rhesus and 6 cynomolgus monkeys (17 male, 4 female) ranging from 3 to 14 years of age were studied. Both eyes were normal in 12 animals, whereas 9 were given laser-induced, unilateral chronic IOP elevations of moderate magnitude (mean, 28 mm Hg; range, 16–38 mm Hg; EEG eye cumulative IOP difference range, 50–807 mm Hg days) and were killed after two confirmations of the CSLT-detected onset of EEG. Optic nerve axon loss in the three EEG eyes in the EEG10-N10 group ranged from 16% to 30%, as previously reported.[6]

Overall Results by Parameter and Group

ALIP was significantly posterior (external) in the EEG compared with N10 eyes of the EEG30/45-N10 group (-36 ± 36 μm vs. -27 ± 27 μm, $P < 0.0001$). *PLIP* was significantly posterior in the EEG compared with N10 eyes of the EEG10/10-N10 (10 ± 41 μm vs. 33 ± 45 μm, $P < 0.0001$) and EEG30/45-N10 (-7 ± 42 μm vs. 37 ± 38 μm, $P < 0.0001$) groups, respectively. Interestingly, *PLIP* within the N30/45 eyes was posterior to the contralateral N10 controls within the N30/45-N10 group (34 ± 35 μm vs. 41 ± 35 μm, $P < 0.0001$), but this difference was substantially less than the differences seen in the EEG eyes. The posterior laminar insertion remained, on average, within the sclera in the N10-N10, N30/45-N10, and EEG10-N10 eyes but exhibited pial insertion within the EEG30/45 eyes (Fig. 5). *LIL* was significantly increased in the EEG eyes of the EEG10-N10 (193 ± 22 μm vs. 161 ± 30 μm, $P < 0.0001$) and EEG30/45-N10 (163 ± 39 μm vs. $131 \pm$

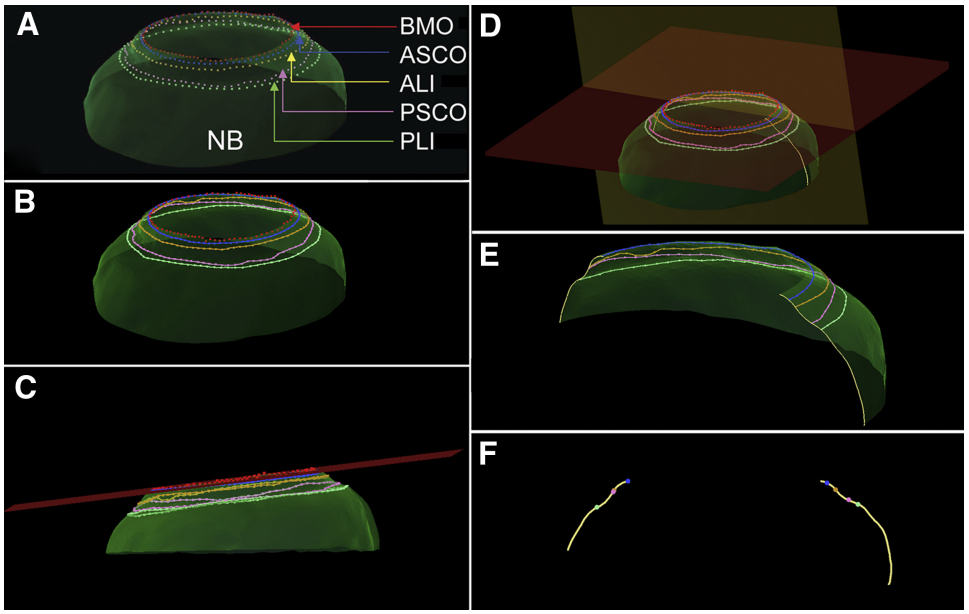

FIGURE 4. Laminar migration and pialization parameters (Fig. 2) are measured within a separate set of 40 digital radial sections of the neural boundary surface and neural canal landmark B-splines acquired relative to the BMO centroid and perpendicular to the BMO reference plane. The most consistent and statistically robust characterization of this anatomy (within and between eyes) is based on equally spaced measurements within true perpendicular sections. Therefore, the initial delineations described in Figure 3 were digitally resampled as follows. (**A**) 3D-delineated neural canal landmark points (Fig. 3) are shown as colored dots on the fitted neural boundary surface (see Fig. 1 for definitions). (**B**) Each set of neural canal landmark points is fit with a smoothed B-spline curve. (**C**) BMO reference plane (*red*) is fit to the 80 BMO landmark points, satisfying a least mean square error as previously described.[9,40] (**D**) To generate the laminar migration and pialization parameters explained in Figure 2, the neural canal landmark B-splines are then sampled using 40 radial digital sagittal sections centered at the BMO centroid and acquired perpendicularly to the BMO reference plane. (**E**) The cut surface of the radial section in (**D**) is shown in the nasal-temporal region of the ONH. (**F**) The isolated neural boundary from the edge of the cut surface is illustrated.

33 μm, $P < 0.0001$) groups, respectively. No significant differences in *Scleral Thickness at ASAS* were noted. See Figure 5 for these results.

Overall Results for Each Parameter by Monkey

ALIP. Overall intereye differences in *ALIP* achieved statistical significance in only one N10-N10 animal (8 μm in magnitude) in N10-N10 animals. *ALIP* was significantly posterior within the EEG eyes of 2 of 3 EEG10 (difference range, 13–14 μm) and 3 of 6 EEG30/45 (difference range, 12–49 μm) animals. Interestingly, *ALIP* was significantly anterior (internal) to that demonstrated by the contralateral N10 eye in a single EEG30/45 eye (monkey EEG4). See Figure 6 for these results.

PLIP. Overall intereye differences in *PLIP* achieved statistical significance in 1 of 6 N10-N10 (17 μm in magnitude) and significance in 3 of 6 N30/45-N10 animals (range, 22–35 μm in magnitude). However the direction of change was not consistent among the three N30/45 eyes that demonstrated this difference. *PLIP* was significantly posterior within the EEG eyes of 2 of 3 EEG10 (difference range, 25–28 μm) and 4 of 6 EEG30/45 (difference range, 46–83 μm) animals, respectively. *PLIP* remained within the sclera within both eyes of the N10-N10, N30/45-N10, and EEG10-N10 groups and achieved pial insertion within the EEG eyes of 4 of 6 EEG30/45-N10 animals (see Fig. 7 for these results).

LIL. Overall intereye differences in *LIL* within the N10-N10 and N30/45-N10 groups achieved significance in 2 of 6 N30/45-N10 monkeys; however, the direction of difference within the N30/45 eyes of these animals (10 μm longer within the N30/45 eye of monkey N11 and 27 μm shorter in the N30/45 eye of monkey N12) was not consistent. *LIL* significantly increased within the EEG eye of all three EEG10-N10 monkeys (range, 31–34 μm) and 4 of 6 EEG30/45-N10 monkeys (range, 30–47 μm; see Fig. 8 for these results).

Scleral Thickness at ASAS

Overall intereye differences in *Scleral Thickness at ASAS* achieved statistical significance in 4 of 6 N10-N10 animals (range, 11–20 μm) and significance in 3 of 6 N30/45-N10 animals (range, 22–36 μm). However, the direction of change was not consistent among the three N30/45 eyes that demonstrated this difference. No EEG10 eye demonstrated a significant decrease in *Scleral Thickness at ASAS.* One EEG eye of the EEG30/45-N10 group (monkey EEG5) demonstrated a significant increase in *Scleral Thickness at ASAS* (39 μm; see Fig. 9 for these results).

FIGURE 5. Overall results by parameter and group. For each parameter, overall between-eye differences within each group were assessed by ANOVA ($P < 0.05$), and statistically significant differences were required to exceed appropriate physiologic intereye differences to be considered biologically important, as described in Materials and Methods. (**A**) *ALIP* (*left*) is plotted relative to the *ASCO* for all four groups *(right). ALIP* posterior migration *(glowing yellow arrow, left*) is suggested in the data for the EEG30/45 eyes (*right*), which is significantly more negative than the data for the contralateral normal eyes. (**B**) *PLIP* (*left*) is plotted relative to the PSCO for all four groups (*right*). *PLIP* posterior migration (*glowing yellow arrow, left*) is suggested in the data for the N30/45, EEG10, and EEG30/45 eyes (*right*), which are all significantly more negative than the data for their contralateral normal eyes. Note that *PLIP* posterior migration in both the EEG10 and EEG10/45 eyes greatly exceeds that demonstrated by the N30/45 eyes (see Discussion). Interestingly, the fact that the mean value for *PLIP* is negative in only the EEG30/45 eyes suggests that *PLIP* remained, on average, within the sclera in the N30/45 and EG 10/10 eyes but involved at least partial pial insertion within the EG30/45 eyes. Note that pialization is denoted within the schematic diagram on the *left* by the fact that the *glowing yellow arrow* extends beyond the PSCO and into the pia. (**C**) An increase in *LIL* (*glowing yellow arrow, left*) was present within the data for the EEG10 and EEG30/45 eyes (*right*) relative to their contralateral normal eyes. (**D**) No significant differences in *Scleral Thickness at ASAS* (*left*) were present in the data for any group (*right*; **D**). All units are micrometers. Data points (*right*) represent the mean ± SD.

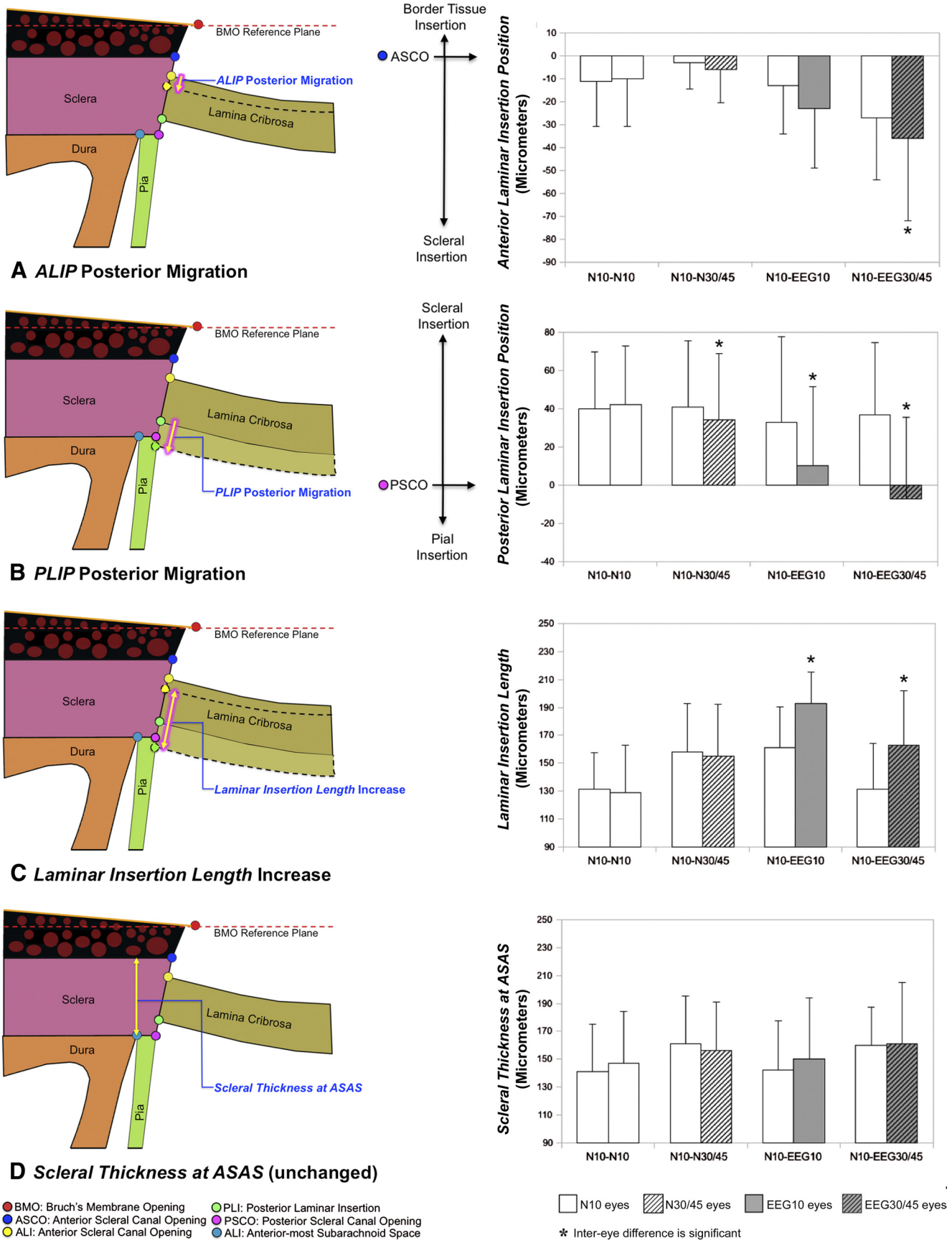
BMO Reference Plane
Sclera
Dura
Pia
Lamina Cribrosa
ALIP Posterior Migration
Border Tissue Insertion
ASCO
Scleral Insertion
Anterior Laminar Insertion Position (Micrometers)
N10-N10
N10-N30/45
N10-EEG10
N10-EEG30/45
A ALIP Posterior Migration
PLIP Posterior Migration
PSCO
Pial Insertion
Posterior Laminar Insertion Position (Micrometers)
B PLIP Posterior Migration
Laminar Insertion Length Increase
Laminar Insertion Length (Micrometers)
C Laminar Insertion Length Increase
Scleral Thickness at ASAS
Scleral Thickness at ASAS (Micrometers)
D Scleral Thickness at ASAS (unchanged)
BMO: Bruch's Membrane Opening
ASCO: Anterior Scleral Canal Opening
ALI: Anterior Scleral Canal Opening
PLI: Posterior Laminar Insertion
PSCO: Posterior Scleral Canal Opening
ALI: Anterior-most Subarachnoid Space
N10 eyes
N30/45 eyes
EEG10 eyes
EEG30/45 eyes
* Inter-eye difference is significant

FIGURE 5.

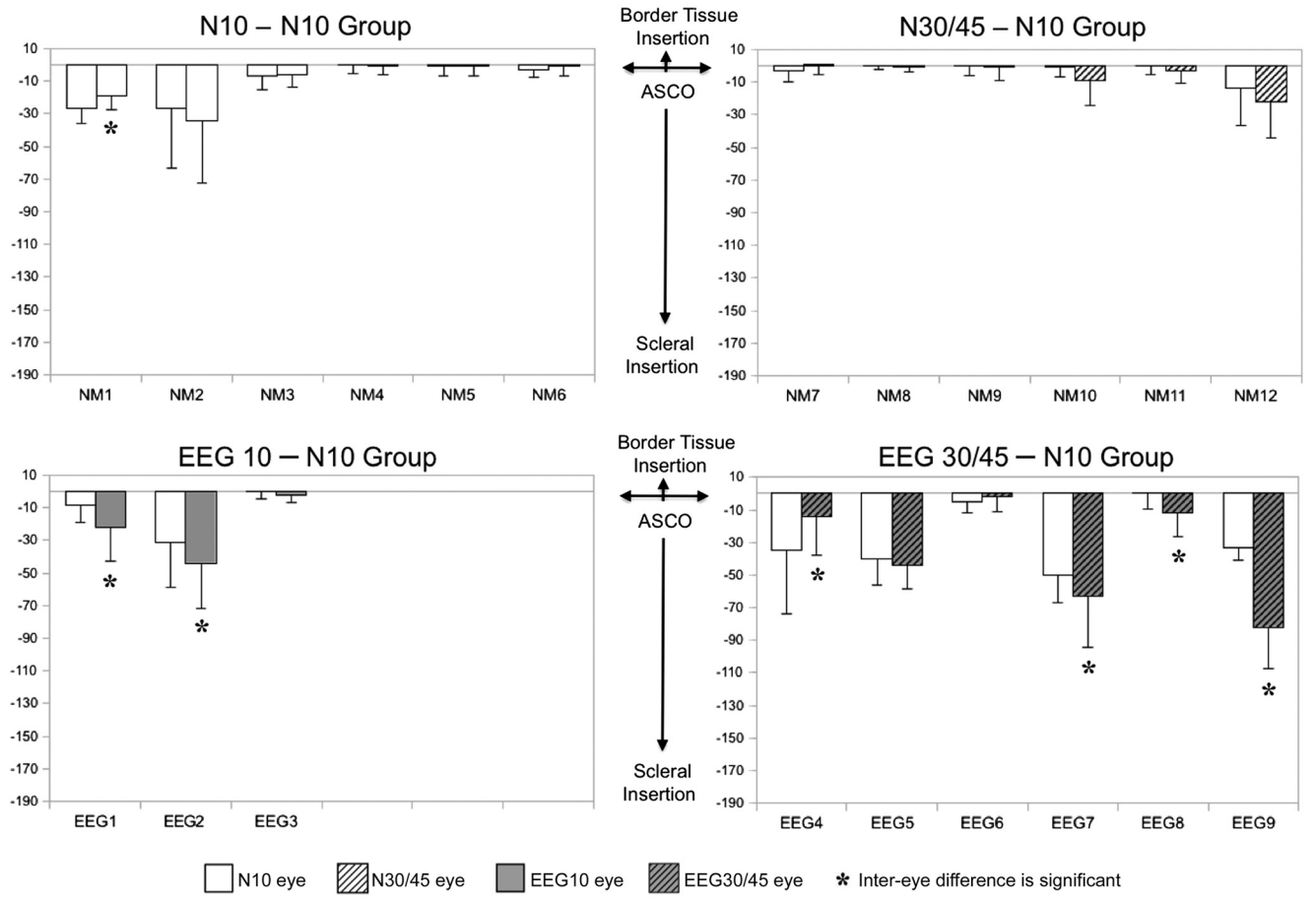

Figure 6. Overall *ALIP* by monkey. Within each monkey, between-eye differences were assessed by ANOVA ($P < 0.05$), and statistically significant differences were required to exceed appropriate physiologic intereye differences to be considered biologically important, as described in Materials and Methods. Based on these criteria, glaucomatous posterior *ALIP* migration was present in 2 of 3 EEG10 eyes and 3 of 6 EEG30/45 eyes. Interestingly, anterior rather than posterior *ALIP* migration appears to be present in the EEG30/45 eye of animal EEG4 (see Discussion). All units are micrometers. Data points represent the mean ± SD.

Discussion

Our study reports postmortem data that suggest progressive posterior migration of the anterior and posterior lamina cribrosa insertions are features of early glaucomatous cupping in the monkey eye. We have previously proposed that a predictable pattern of anterior to posterior mechanical failure of the laminar beams likely underlies the pathophysiology of glaucomatous cupping.[6,7] More recently, we adjusted this concept to include the notion that the lamina cribrosa is thickened[5,8] at the stage at which a loss of anterior beams can be detected. We then used finite element modeling techniques to detect the presence of additional laminar beams within the thickened lamina and suggested that active recruitment of the retrolaminar septa into more horizontally oriented tissues was one mechanism by which this thickening might have occurred.[22]

The fact that the anterior laminar insertion demonstrates posterior migration in early experimental glaucoma is important for the following reasons. First, whether it is the result of physical disruption[7] or remodeling,[15–17,22] the finding of anterior laminar insertion migration in our study strongly suggested a loss of identifiable anterior laminar beams. Such a loss, where present, is counter to the predictions of current microstructure-motivated growth and remodeling engineering algorithms,[27] which predict that the lamina's response to chronic IOP elevation will be thickening through both anterior (inward) migration of the anterior laminar insertion and posterior (outward) migration of the posterior laminar insertion. It is not necessary for the anterior laminar insertion to migrate for the lamina to thicken. Taken together, posterior migration of the anterior laminar insertion is most likely the result of primary damage to the anterior laminar beam insertions or of the damage that occurs during their unsuccessful or disrupted remodeling. Its location provides plausible mechanisms for both retinal nerve fiber hemorrhages[24,43] and glaucomatous excavation of the neural canal wall beneath the Bruch's membrane opening and the anterior scleral canal opening.[3,19]

In the context of this discussion, it is interesting that one of the EEG30/45-N10 animals (EEG4) demonstrated significant anterior rather than posterior migration of the anterior laminar insertion in the EEG30/45 eye (Fig. 6) without demonstrating significant posterior laminar insertion migration (Fig. 7) or laminar insertion thickening (Fig. 8). Regional analyses of these phenomena and how they colocalize in all 9 EEG eyes are pending.

Although the anterior laminar beams insert directly into the sclera in most monkey eyes, in some they regionally insert high into the border tissues of Elschnig (CFB, personal observation, 2011). Primary trauma to or remodeling of the anterior laminar beam capillaries or their border tissue insertion sites would occur at the most common clinical location of nerve fiber layer hemorrhages and provide leaking blood direct access to the most peripheral RGC axon bundles.[24,43]

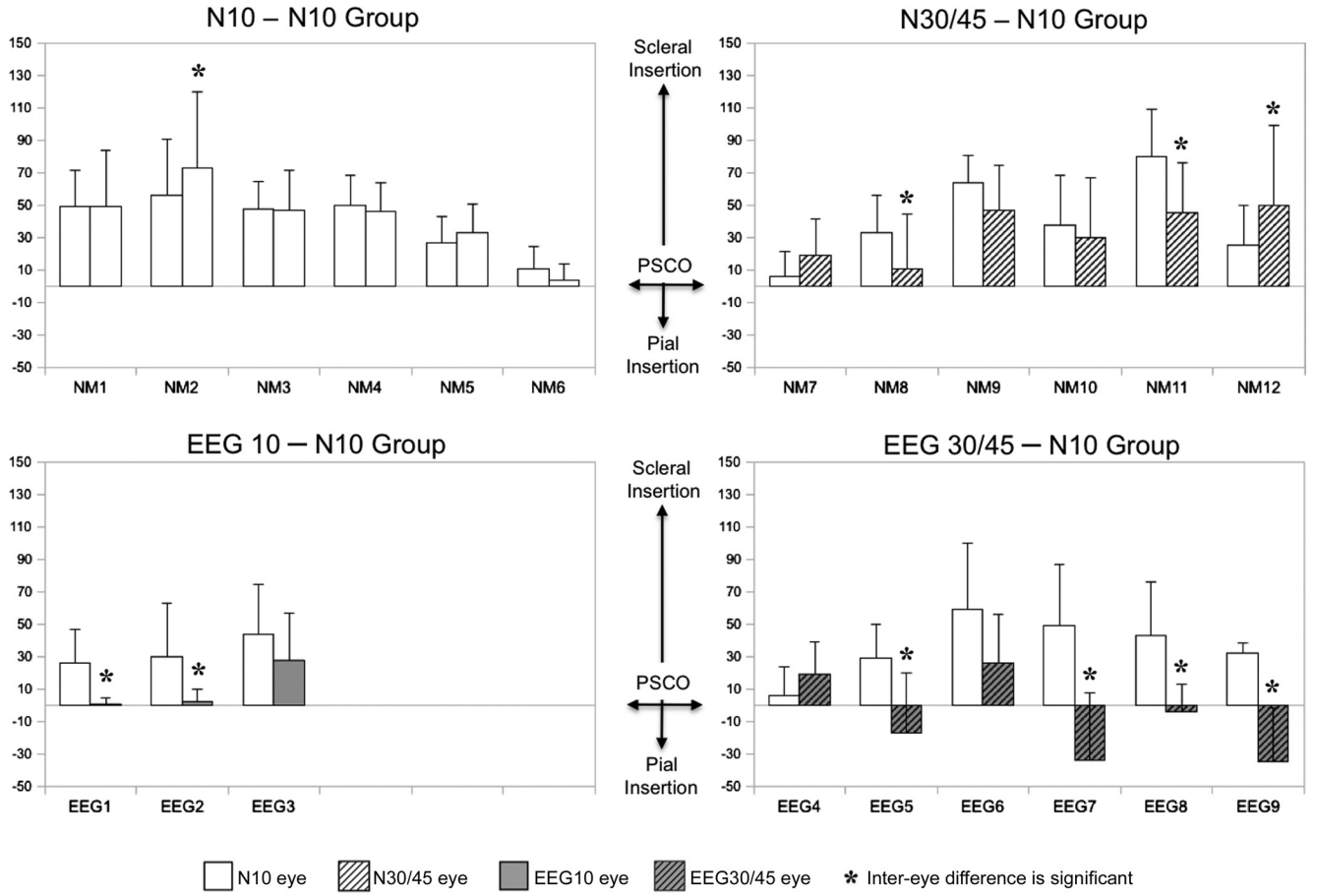

FIGURE 7. Overall *PLIP* by monkey. Within each monkey, between-eye differences were assessed by ANOVA ($P < 0.05$), and statistically significant differences were required to exceed appropriate physiologic intereye differences to be considered biologically important, as described in Materials and Methods. Based on these criteria, glaucomatous posterior *PLIP* migration was present in 2 of 3 EEG10 eyes and 4 of 6 EEG30/45 eyes. *PLIP* remained, on average, within the sclera within the N10, N30/45, and EEG10 eyes and involved at least partial pial insertion within the 4 of 6 EEG30/45 eyes that achieved significance. All units are micrometers. Data points represent the mean ± SD.

Similarly, posterior migration of the anterior laminar insertion should reduce the laminar portion of the scleral canal's resistance to radial expansion and may, therefore, be a contributing mechanism for the clinical phenomenon of glaucomatous excavation.[3,7,18,19] We have previously reported regional scleral canal expansion in most of the nine EEG eyes of this study and have discussed the relationship of this finding to the literature on excavation.[12]

Our working hypothesis to link laminar insertion migration, laminar thickening,[8,11] and retrolaminar septal recruitment into the laminar structure[22] was that the early onset of focal anterior laminar beam failure would decrease the connective tissues available to resist IOP and thereby increase the stresses within the remaining beams driving posterior laminar insertion migration and retrolaminar septal recruitment.[5,22] However, our overall data suggest that outward migration of the posterior laminar insertion (migration distance range, 25–83 μm individually) exceeded that of the anterior laminar insertion (migration distance range, 12–49 μm individually) in most of the EEG eyes. One interpretation of the fact that the magnitude of posterior laminar insertion migration exceeds the magnitude of anterior laminar insertion is that posterior laminar insertion migration may not be a response to anterior laminar insertion migration but, in fact, may precede it. The results reported herein are cross-sectional in nature and, therefore, cannot address this question. Hence, longitudinal detection of these laminar migration phenomena using 870 and 1050 nm wavelength SD-OCT imaging is now being attempted in our laboratory.

It is entirely plausible that the lamina's response to elevated IOP is to change shape[6,8,11,44] (Sigal IA, et al. *IOVS* 2009;50: ARVO E-Abstract 4888), change laminar beam thickness regionally (Grimm J, et al. *IOVS* 2007;48:ARVO E-Abstract 3295), and recruit the connective tissues of the retrolaminar septa into a more horizontal configuration through the active process of connective tissue remodeling.[17,22] Thickening of the lamina within the sclera with eventual extension into the pial sheaths would be predicted postmortem markers of these events. Future longitudinal studies, using in vivo imaging modalities designed to image the lamina cribrosa beams at their peripheral insertion[38,39,45] (Park SC, et al. *IOVS* 2011;52:ARVO E-Abstract 3063) will be required to characterize the actual onset, progression, and interaction of these phenomena.

It is important to note we detected significantly anterior ($n = 1$) and posterior ($n = 2$) *PLIP* values in the high IOP eye in 3 of 6 N30/45-N10 animals (intereye difference range, +22 to −35 μm). This finding made it necessary to require that statistically significant intereye differences within the six EEG30/45-N10 animals exceed 35 μm in magnitude to achieve biological importance. Because we propose that laminar migration is a slowly progressive pathophysiologic phenomenon, we do not believe that actual migration of the posterior laminar insertion occurred during the 30 minutes of acute IOP elevation in the two N30/45 eyes that demonstrated this difference.

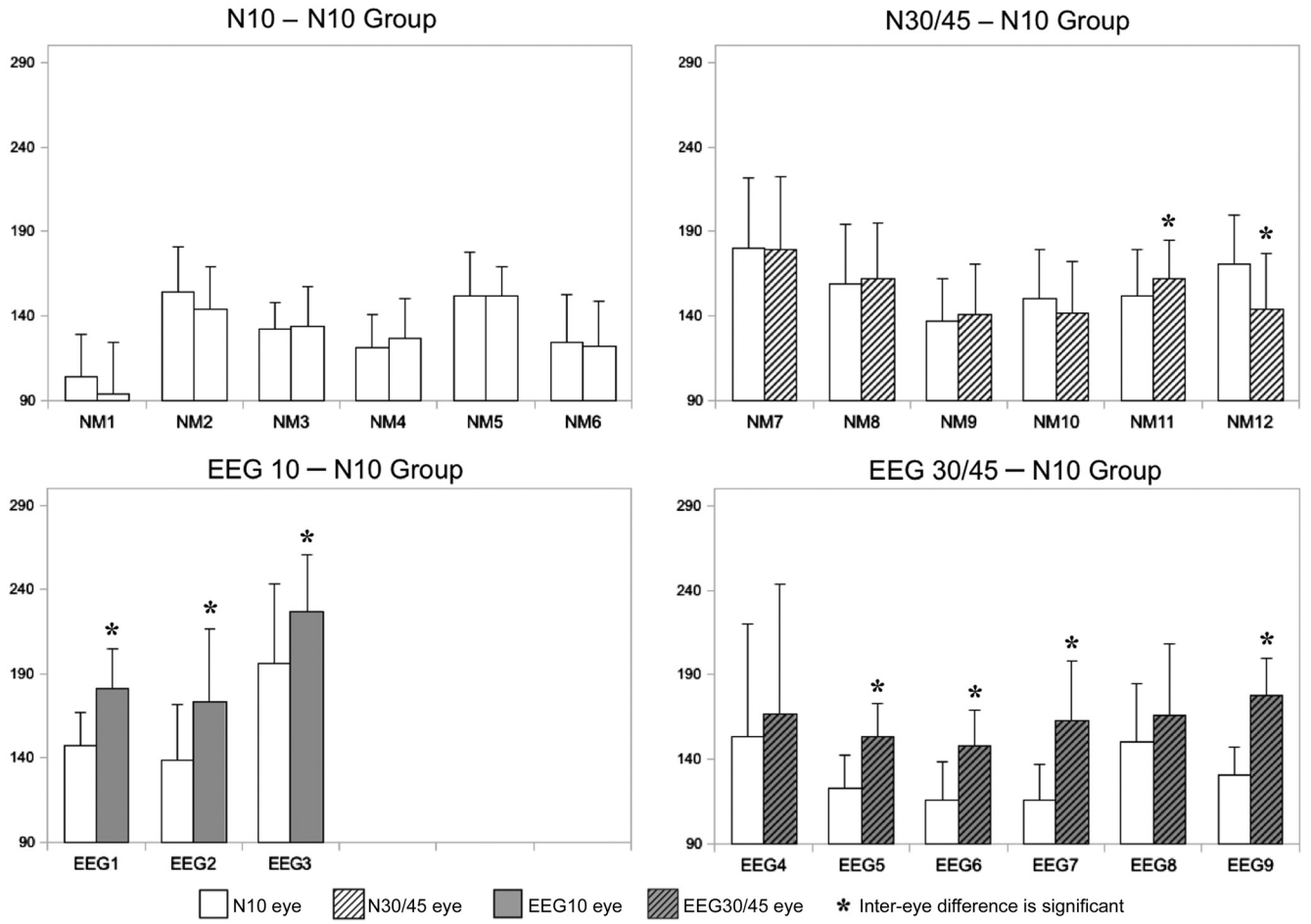

Figure 8. Overall *LIL* by monkey. Within each monkey, between-eye differences were assessed by ANOVA ($P < 0.05$), and statistically significant differences were required to exceed appropriate physiologic intereye differences to be considered biologically important, as described in Materials and Methods. Based on these criteria, glaucomatous increases in *LIL* were present in 3 of 3 EEG10 eyes and 4 of 6 EEG30/45 eyes. Interestingly, no EEG eye decreases in *LIL* were noted. All units are micrometers. Data points represent the mean and SD.

Instead, we believe this finding in a subset of the N30/45-N10 animals represents an expansion of the physiologic intereye difference magnitude for this parameter[14] beyond that established by the N10-N10 group of animals. This explanation is supported by the lack of a consistent direction within the N30/45 eyes of the three N30/45-N10 animals that demonstrated this difference. However, the presence of significant differences within the N30/45-N10 animals (Fig. 5) suggests that an acute IOP elevation-induced measurement effect on this parameter may be present and remains to be determined.

Several authors have previously described phenomena that we believe are related to laminar migration and pialization in normal and glaucomatous human eyes, although they did not describe it in these terms. First, Sigal et al.[46] described partial lamina cribrosa insertion into the pial sheath in normal human cadaver eyes; this finding has been confirmed by a separate 3D histomorphometric study (Girkin CA, et al. *IOVS* 2010;51:ARVO E-Abstract 3854). This finding may reflect a fundamental species-specific difference in ONH connective tissue architecture if it is present at all ages. However, we believe that this is likely to be most common in the aged eye and that age-related laminar remodeling and glaucomatous laminar remodeling may, therefore, overlap. Interestingly, Hogan and Zimmerman[47] described age-related thickening of the retrolaminar connective tissue septa and assumed it to follow age-related axon loss. Whether thickened retrolaminar septa are present and contain more transverse-oriented fibers that insert into the pia in eyes of older monkeys and of humans is a topic under study within our collaborative group and will be the subject of future reports.

In a separate finite element study that used individual-specific models of normal human cadaver eyes, Sigal et al.[48] reported that the retrolaminar pia was more robustly load bearing than expected. Although they did not specifically comment that the lamina inserted into the regions of pial thickening, pial thickening would be the predicted result of an extended period in which the lamina transferred load.

Jonas[49] has suggested that an alteration in the translaminar pressure gradient within the peripheral nerve is one consequence of glaucomatous cupping. Prelaminar neural tissue thinning and anterior laminar insertion migration should both shorten the distance from the Internal Limiting Membrane to the Anterior-most Subarachnoid Space. For given levels of IOP and cerebrospinal fluid pressure, shortening this distance should increase the steepness of the gradient within the remaining tissues. Although we have previously reported prelaminar neural tissue thickening rather than thinning at this stage of the neuropathy,[6] future studies will include measures of minimum Internal Limiting Membrane to Anterior-most Subarachnoid Space distance.

Hayreh et al.[50] have reported retrolaminar fibrosis in the monkey model of experimental glaucoma in a qualitative 2D histologic study. This observation is compatible with our hypothesis of thickening and recruitment of retrolaminar septa into the load-bearing laminar structure, though no comment

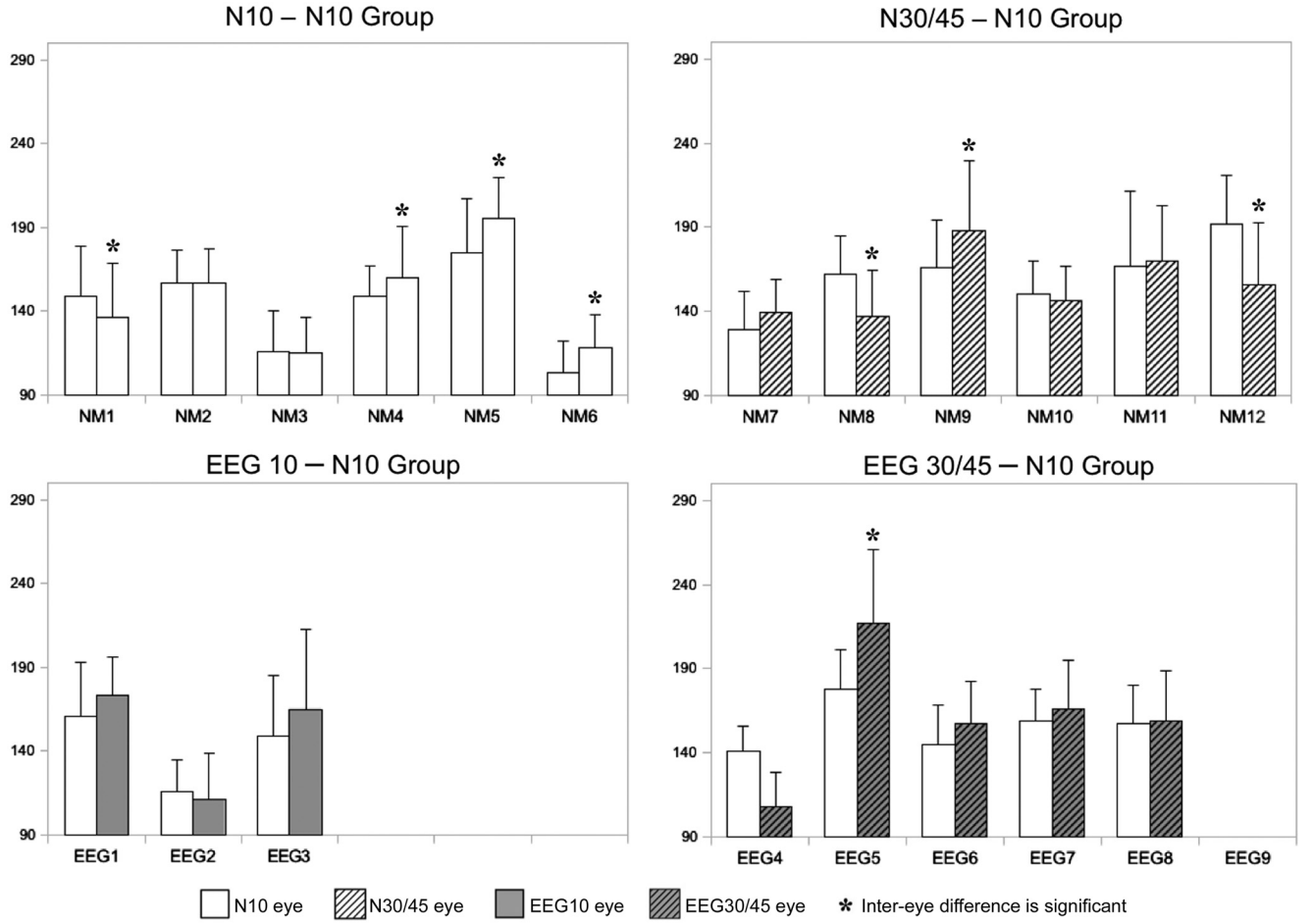

FIGURE 9. Overall *Scleral Thickness at ASAS* by monkey. Within each monkey, between-eye differences were assessed by ANOVA ($P < 0.05$), and statistically significant differences were required to exceed appropriate physiologic intereye differences to be considered biologically important, as described in Materials and Methods. Based on these criteria, glaucomatous alterations in *Scleral Thickness at ASAS* were present in 0 of 3 EEG10 eyes and only 1 of 6 EEG30/45 eyes (an increase in EEG5). All units are micrometers. Data points represent the mean and SD.

was made about the orientation of beams or their insertion into the pia. Of note, the animals in that study[50] had more advanced glaucomatous damage; hence, retrolaminar fibrosis could be expected on the basis of advanced axon loss alone.

The limitations of our study and methods have been extensively discussed in a series of previous publications.[6,8,9,12–14] They are noted briefly as follows. Our study includes 15 rhesus and 6 cynomolgus monkeys (Table 2), which may confound our results. Although there may be species differences in monkey ONH architecture and material properties that could influence their response to both chronic and acute IOP elevation,[10,11,51] we doubt these are important in our study for the following reasons. First, there are no obvious differences between the normal eye measurements for the two species.[6,8,9,12–14] Second, there is no clear separation of the two species when we ordered overall deformations in the nine EEG eyes.[12]

Second, our delineators were not masked to the IOP and kill condition of each delineated eye during the delineation. Although it is possible they were biased in the delineation of the ONH landmarks on this basis, we believe this is unlikely because these eyes were delineated >2 years before we formulated our hypotheses regarding the presence of posterior laminar migration in the early glaucoma eyes, and the delineators were completely unaware of these concepts and ideas at the time of delineation.

Finally, because of the fundamental differences in the geometry and material properties of the ONH and peripapillary sclera between monkey and human eyes, our findings may have limited application to the human eye. Although human sclera is 2 to 4 times thicker than monkey sclera,[51–53] direct comparison of scleral material properties using the same testing apparatus and modeling strategy is in process but is not yet completed. The human lamina cribrosa (119–463 μm)[18,46] is also thicker than the monkey lamina (117–210 μm).[6,8,12–14] Laminar material properties in both species are at present unknown. Taken together, the human lamina and sclera may be more robust in their young normal state and, therefore, less likely to recruit septa and or to migrate in response to elevated IOP and aging.

In summary, these postmortem data support the hypothesis that progressive posterior migration of the lamina cribrosa from the sclera toward the pia is a component of early cupping in monkey experimental glaucoma. Our data specifically suggest that at the onset of CSLT-detected ONH surface change in monkeys exposed to chronic, moderate, unilateral, laser-induced IOP elevations, most EEG eyes demonstrate posterior migration of the anterior and posterior lamina cribrosa insertions that achieve at least partial pialization in a subset of eyes. The regional consistency of these phenomena and their contributions to the mechanisms of glaucomatous damage to the adjacent astrocytes, glia, and retinal ganglion cell axons[23] are

under study. However, because our postmortem data are by definition cross-sectional, longitudinal characterization of the onset and progression of laminar migration in monkey EEG is now necessary.

Acknowledgments

The authors thank the following for their assistance in this study: Jonathan Grimm and Juan Reynaud for assistance with software and hardware, Erica Dyrud for assistance with delineation, Pris Zhou and Anthony Bellezza, for their work of animal testing, and Joanne Couchman and Jinjing Qi for their assistance with manuscript preparation and submission.

References

1. Pederson JE, Anderson DR. The mode of progressive disc cupping in ocular hypertension and glaucoma. *Arch Ophthalmol.* 1980;98:490–495.
2. Vrabec F. Glaucomatous cupping of the human optic disk: a neuro-histologic study. *Albrecht Von Graefes Arch Klin Exp Ophthalmol.* 1976;198:223–234.
3. Quigley HA, Green WR. The histology of human glaucoma cupping and optic nerve damage: clinicopathologic correlation in 21 eyes. *Ophthalmology.* 1979;86:1803–1830.
4. Trobe JD, Glaser JS, Cassady J, Herschler J, Anderson DR. Nonglaucomatous excavation of the optic disc. *Arch Ophthalmol.* 1980;98:1046–1050.
5. Burgoyne CF, Downs JC. Premise and prediction—how optic nerve head biomechanics underlies the susceptibility and clinical behavior of the aged optic nerve head. *J Glaucoma.* 2008;17:318–328.
6. Yang H, Downs JC, Bellezza AJ, Thompson H, Burgoyne CF. 3D histomorphometry of the normal and early glaucomatous monkey optic nerve head: prelaminar neural tissues and cupping. *Invest Ophthalmol Vis Sci.* 2007;48:5068–5084.
7. Burgoyne CF, Downs JC, Bellezza AJ, Suh JK, Hart RT. The optic nerve head as a biomechanical structure: a new paradigm for understanding the role of IOP-related stress and strain in the pathophysiology of glaucomatous optic nerve head damage. *Prog Retin Eye Res.* 2005;24:39–73.
8. Yang H, Downs JC, Girkin C, et al. 3D Histomorphometry of the normal and early glaucomatous monkey optic nerve head: lamina cribrosa and peripapillary scleral position and thickness. *Invest Ophthalmol Vis Sci.* 2007;48:4597–4607.
9. Downs JC, Yang H, Girkin C, et al. 3D histomorphometry of the normal and early glaucomatous monkey optic nerve head: neural canal and subarachnoid space architecture. *Invest Ophthalmol Vis Sci.* 2007;48:3195–3208.
10. Burgoyne CF, Downs JC, Bellezza AJ, Hart RT. Three-dimensional reconstruction of normal and early glaucoma monkey optic nerve head connective tissues. *Invest Ophthalmol Vis Sci.* 2004;45:4388–4399.
11. Bellezza AJ, Rintalan CJ, Thompson HW, Downs JC, Hart RT, Burgoyne CF. Deformation of the lamina cribrosa and anterior scleral canal wall in early experimental glaucoma. *Invest Ophthalmol Vis Sci.* 2003;44:623–637.
12. Yang H, Thompson H, Roberts MD, Sigal IA, Downs JC, Burgoyne CF. Deformation of the early glaucomatous monkey optic nerve head connective tissue after acute IOP elevation in 3D histomorphometric reconstructions. *Invest Ophthalmol Vis Sci.* 2011;52:345–363.
13. Yang H, Downs JC, Sigal IA, Roberts MD, Thompson H, Burgoyne CF. Deformation of the normal monkey optic nerve head connective tissue after acute IOP elevation within 3D histomorphometric reconstructions. *Invest Ophthalmol Vis Sci.* 2009;50:5785–5799.
14. Yang H, Downs JC, Burgoyne CF. Physiologic intereye differences in monkey optic nerve head architecture and their relation to changes in early experimental glaucoma. *Invest Ophthalmol Vis Sci.* 2009;50:224–234.
15. Hernandez MR. The optic nerve head in glaucoma: role of astrocytes in tissue remodeling. *Prog Retin Eye Res.* 2000;19:297–321.
16. Hernandez MR, Ye H. Glaucoma: changes in extracellular matrix in the optic nerve head. *Ann Med.* 1993;25:309–315.
17. Downs JC, Roberts MD, Sigal IA. Glaucomatous cupping of the lamina cribrosa: a review of the evidence for active progressive remodeling as a mechanism. *Exp Eye Res*. First published on 11 August 2010 as doi:10.1016/j.exer.2010.08.004.
18. Quigley HA, Hohman RM, Addicks EM, Massof RW, Green WR. Morphologic changes in the lamina cribrosa correlated with neural loss in open-angle glaucoma. *Am J Ophthalmol.* 1983;95:673–691.
19. Quigley HA, Addicks EM, Green WR, Maumenee AE. Optic nerve damage in human glaucoma, II: the site of injury and susceptibility to damage. *Arch Ophthalmol.* 1981;99:635–649.
20. Agapova OA, Kaufman PL, Lucarelli MJ, Gabelt BT, Hernandez MR. Differential expression of matrix metalloproteinases in monkey eyes with experimental glaucoma or optic nerve transection. *Brain Res.* 2003;967:132–143.
21. Roberts MD, Sigal IA, Liang Y, Burgoyne CF, Downs JC. Changes in the biomechanical response of the optic nerve head in early experimental glaucoma. *Invest Ophthalmol Vis Sci.* 2010;51:5675–5684.
22. Roberts MD, Grau V, Grimm J, et al. Remodeling of the connective tissue microarchitecture of the lamina cribrosa in early experimental glaucoma. *Invest Ophthalmol Vis Sci.* 2009;50:681–690.
23. Burgoyne CF. A biomechanical paradigm for axonal insult within the optic nerve head in aging and glaucoma. *Exp Eye Res*. First published on 16 September 2010 as doi:10.1016/j.exer.2010.09.005.
24. Jonas JB, Xu L. Optic disk hemorrhages in glaucoma. *Am J Ophthalmol.* 1994;118:1–8.
25. Siegner SW, Netland PA. Optic disc hemorrhages and progression of glaucoma [see comments]. *Ophthalmology.* 1996;103:1014–1024.
26. Pena JD, Agapova O, Gabelt BT, et al. Increased elastin expression in astrocytes of the lamina cribrosa in response to elevated intraocular pressure. *Invest Ophthalmol Vis Sci.* 2001;42:2303–2314.
27. Grytz R, Sigal IA, Ruberti JW, Meschke G, Downs JC. Lamina cribrosa thickening in early glaucoma predicted by a microstructure motivated growth and remodeling approach. *Int J Mech Mater.* In press.
28. Cioffi GA, Van Buskirk EM. *Vasculature of the Anterior Optic Nerve and Peripapillary Choroid*. 2nd ed. St. Louis: Mosby; 1996:177–197.
29. Jonas JB, Berenshtein E, Holbach L. Lamina cribrosa thickness and spatial relationships between intraocular space and cerebrospinal fluid space in highly myopic eyes. *Invest Ophthalmol Vis Sci.* 2004;45:2660–2665.
30. Jonas JB. Trans-lamina cribrosa pressure difference. *Arch Ophthalmol.* 2007;125:431, author reply 431.
31. Ren R, Jonas JB, Tian G, et al. Cerebrospinal fluid pressure in glaucoma: a prospective study. *Ophthalmology.* 2010;117:259–266.
32. Morgan WH, Yu DY, Cooper RL, Alder VA, Cringle SJ, Constable IJ. The influence of cerebrospinal fluid pressure on the lamina cribrosa tissue pressure gradient. *Invest Ophthalmol Vis Sci.* 1995;36:1163–1172.
33. Morgan WH, Yu DY, Alder VA, et al. The correlation between cerebrospinal fluid pressure and retrolaminar tissue pressure. *Invest Ophthalmol Vis Sci.* 1998;39:1419–1428.
34. Bussow H. The astrocytes in the retina and optic nerve head of mammals: a special glia for the ganglion cell axons. *Cell Tissue Res.* 1980;206:367–378.
35. Morgan JE. Optic nerve head structure in glaucoma: astrocytes as mediators of axonal damage. *Eye.* 2000;14(pt 3B):437–444.
36. Shirakashi M. The effects of intraocular pressure elevation on optic nerve axonal transport in the monkey. *Acta Ophthalmol.* 1990;68:37–43.
37. Quigley HA, Guy J, Anderson DR. Blockade of rapid axonal transport: effect of intraocular pressure elevation in primate optic nerve. *Arch Ophthalmol.* 1979;97:525–531.
38. Inoue R, Hangai M, Kotera Y, et al. Three-dimensional high-speed optical coherence tomography imaging of lamina cribrosa in glaucoma. *Ophthalmology.* 2009;116:214–222.

39. Srinivasan VJ, Adler DC, Chen Y, et al. Ultrahigh-speed optical coherence tomography for three-dimensional and en face imaging of the retina and optic nerve head. *Invest Ophthalmol Vis Sci.* 2008;49:5103–5110.
40. Zawadzki RJ, Choi SS, Fuller AR, Evans JW, Hamann B, Werner JS. Cellular resolution volumetric in vivo retinal imaging with adaptive optics-optical coherence tomography. *Opt Express.* 2009;17:4084–4094.
41. Strouthidis NG, Yang H, Fortune B, Downs JC, Burgoyne CF. Detection of optic nerve head neural canal opening within histomorphometric and spectral domain optical coherence tomography data sets. *Invest Ophthalmol Vis Sci.* 2009;50:214–223.
42. Edwards D, Berry JJ. The efficiency of simulation-based multiple comparisons. *Biometrics.* 1987;43:913–928.
43. Airaksinen PJ, Mustonen E, Alanko HI. Optic disc hemorrhages: analysis of stereophotographs and clinical data of 112 patients. *Arch Ophthalmol.* 1981;99:1795–1801.
44. Sigal IA, Yang H, Roberts MD, Burgoyne CF, Downs JC. Biomechanics of the posterior pole during remodeling progression from normal to early experimental glaucoma. *ASME.* Summer Bioengineering Conference; June 17–21, 2009; Lake Tahoe.
45. Agoumi Y, Sharpe GP, Hutchison DM, Nicolela MT, Artes PH, Chauhan BC. Laminar and prelaminar tissue displacement during intraocular pressure elevation in glaucoma patients and healthy controls. *Ophthalmology.* 2011;118:52–59.
46. Sigal IA, Flanagan JG, Tertinegg I, Ethier CR. 3D Morphometry of the human optic nerve head. *Exp Eye Res.* 2010;90:70–80.
47. Hogan MJ, Zimmerman LE. The optic nerve. In: Hogan MJ, Zimmerman LE, eds. *Ophthalmic Pathology*. Philadelphia: WB Saunders; 1969:577–590.
48. Sigal IA, Flanagan JG, Tertinegg I, Ethier CR. Modeling individual-specific human optic nerve head biomechanics, II: influence of material properties. *Biomech Model Mechanobiol.* 2009;8:99–109.
49. Jonas JB, Berenshtein E, Holbach L. Anatomic relationship between lamina cribrosa, intraocular space, and cerebrospinal fluid space. *Invest Ophthalmol Vis Sci.* 2003;44:5189–5195.
50. Hayreh SS, Pe'er J, Zimmerman MB. Morphologic changes in chronic high-pressure experimental glaucoma in rhesus monkeys. *J Glaucoma.* 1999;8:56–71.
51. Downs JC, Blidner RA, Bellezza AJ, Thompson HW, Hart RT, Burgoyne CF. Peripapillary scleral thickness in perfusion-fixed normal monkey eyes. *Invest Ophthalmol Vis Sci.* 2002;43:2229–2235.
52. Norman RE, Flanagan JG, Rausch SM, et al. Dimensions of the human sclera: thickness measurement and regional changes with axial length. *Exp Eye Res.* 2010;90:277–284.
53. Downs JC, Ensor ME, Bellezza AJ, Thompson HW, Hart RT, Burgoyne CF. Posterior scleral thickness in perfusion-fixed normal and early-glaucoma monkey eyes. *Invest Ophthalmol Vis Sci.* 2001;42:3202–3208.